PRECLINICAL AND CLINICAL IMAGING - Full Papers

Magnetic Resonance in Medicine 68:234–240 (2012)

In Vivo Detection of Excitotoxicity by Manganese-Enhanced MRI: Comparison with Physiological Stimulation

Oliviero L. Gobbo,[1–4] Fanny Petit,[2,3] Hirac Gurden,[5*] and Marc Dhenain[2–4*]

Manganese-enhanced MRI (MEMRI) is a powerful technique for the in vivo monitoring of brain function in animals. Manganese enters into cells through calcium channels, i.e., voltage-gated calcium channels and activated glutamate receptors (e.g., *N*-methyl-D-aspartate receptors). *N*-methyl-D-aspartate receptors are activated both in normal physiological and pathophysiological conditions. Consistent with these mechanisms, we showed that in the olfactory bulb, the MEMRI signal strongly increases when excitotoxic mechanisms are induced by an administration of a *N*-methyl-D-aspartate receptor agonist, quinolinate. We found that the intensity of the MEMRI signal in excitotoxic conditions is similar to the odor-evoked signal in normal physiological conditions. Finally, we showed that the dynamics of the MEMRI signal are determined by the early phase of manganese in the olfactory bulb. Overall, these data show that, in addition to physiological studies, MEMRI can be used as an in vivo method to follow-up the dynamics of excitotoxic events. Magn Reson Med 68:234–240, 2012.

Key words: manganese; magnetic resonance imaging; excitotoxicity; quinolinate; olfaction; rat

Manganese (Mn^{2+}) enhanced magnetic resonance imaging (MEMRI) is widely used for brain exploration. This method relies on the complementary properties of Mn^{2+}: First, it is a paramagnetic ion that affects the T1 relaxivity (1); second, it is a Ca^{2+} analogue that can enter both neurons (2); and glial cells (3); and third, it can be transported along axons, can cross synapses and enter postsynaptic cells. These characteristics make it useful to improve contrast in MRI to evaluate, in fine detail, brain architectures (4), track transplanted cells (5), and trace fibre tracts (2,6). Finally, the last major application of MEMRI is to highlight activated regions in the brain (7,8). This latter application is related to the ability of Mn^{2+} to enter into activated cells after its systemic or intracerebral administration. Indeed, during physiological neuronal activation, extracellular Mn^{2+}, as an analogue of calcium, enters neurons mainly through *N*-methyl-D-aspartate (NMDA) receptors (9) and voltage-gated calcium channels (VGCC) (10). Activity-dependent Mn^{2+} uptake can thus map focal active regions within sensory systems (8,10,11).

In addition to their physiological roles in cellular activation, NMDA receptors also play a crucial role in pathological excitotoxic mechanisms. Excitotoxicity is defined as excessive exposure to the neurotransmitter glutamate or over-stimulation of its postsynaptic membrane receptors, leading to neuronal injury or death (12). It occurs in most brain injury processes both in acute alteration (for example, in stroke) or slowly evolving pathologies (for example, in the case of Alzheimer's disease) (12). It is thus a critical event that is widely studied by neurobiologists. In experimental conditions, excitotoxic events can be mimicked by the use of various drugs such as the NMDA receptor agonist quinolinate (13–15). The role of ionotropic (NMDA-subtype) and metabotropic glutamate receptors (15) in quinolinate-excitotoxic events is mediated by the disruption of intracellular calcium homeostasis that leads to cell death cascades (16). Because the Mn^{2+}-dependent signal enhancement is mainly triggered by glutamate receptors (9,15), it should be possible to visualize how MEMRI signals vary during the excitotoxic processes.

The aim of this study was to assess the MEMRI signals during a pathological, excitotoxic situation and to compare it to the MEMRI signal in physiological conditions. We used the olfactory bulb (OB) as a model system to tackle this question because after intranasal administration, Mn^{2+} can directly reach the OB thus making the imaging of odor activation possible (17). Therefore, we compared the MEMRI signal intensity after odor stimulation (functional condition) or quinolinate activation (excitotoxic condition) in the OB of rats. We showed that quinolinate-induced activity is reliably detected by MEMRI and physiological stimulation can induce MEMRI signal modifications that are similar to the lesioned tissue in terms of intensity and dynamics.

MATERIALS AND METHODS

Subjects

Thirty-two male Sprague-Dawley rats (300 g) were involved in the MEMRI study. They were randomly

[1]School of Pharmacy and Pharmaceutical Sciences, and Trinity College Institute of Neuroscience, Trinity College Dublin, Dublin 2, Ireland.

[2]CNRS, URA 2210, 18 route du panorama, 92 265 Fontenay-aux-Roses cedex, France.

[3]CEA, DSV, I2BM, MIRCen, URA CEA CNRS 2210, 18 route du panorama, 92 265 Fontenay-aux-Roses cedex, France.

[4]CEA, DSV, I2BM, NeuroSpin, Centre CEA de Saclay, Bât. 145, 91191 Gif sur Yvette, France.

[5]CNRS, UMR8165, Universités P7-P11, Bat440, Université Paris-Sud, 91405 Orsay Cedex, France.

Grant sponsor: National Institute on Aging; Grant number: R01-AG020197; Grant sponsors: Higher Education Authority Programme for Research in Third-Level Institutions, France-Alzheimer Association.

*Correspondence to: Marc Dhenain, DVM, PhD, MIRCen, URA CEA CNRS 2210, 18 route du panorama 92265 Fontenay-aux-Roses cedex, France. E-mail: Marc.Dhenain@cea.fr or Hirac Gurden, PhD, CNRS, UMR8165, Université s P7-P11, Bat440, Université Paris-Sud, 91405 Orsay Cedex, France.

Received 26 April 2011; revised 27 July 2011; accepted 17 August 2011.

DOI 10.1002/mrm.23210

Published online 29 November 2011 in Wiley Online Library (wileyonlinelibrary.com).

Table 1
MEMRI Protocol

				Day 3		
		Day 1	Day 2	T_0	$t_0 + 10$ min	$t_0 + 90$ min
Physiological conditions	Control ($n = 6$)	Baseline MRI	–	$MnCl_2$	–	MEMRI
	"Odor-stim" ($n = 5$)	Baseline MRI	–	$MnCl_2$	Odor	MEMRI
Pathological conditions	Sham ($n = 7$)	Baseline MRI	Surgery, saline	$MnCl_2$	–	MEMRI
	"Quino45" ($n = 6$)	Baseline MRI	Surgery, quinolinate 45 mM	$MnCl_2$	–	MEMRI
	"Quino90" ($n = 6$)	Baseline MRI	Surgery, quinolinate 90 mM	$MnCl_2$	–	MEMRI

Day 1: all animals were anesthetized and imaged by T1-weighted MRI. Day 2: rats were anesthetized and injected into the OB with either saline (sham group) or quinolinate at 45 mM (quino45) or 90 mM (quino90). Day 3: intranasal $MnCl_2$ (5 μL, 1 M) injection was performed in all animals and the physiological activation was triggered by odor presentation in the "odor-stim" group. Locations of manganese were detected by MRI in all groups imaged 90 to 200 min following $MnCl_2$ injection.

assigned to one of the five following experimental groups: control animals without any stimulation or surgery (control, $n = 6$); animals exposed to odor (amylacetate) stimulation (odor-stim, $n = 5$); animals injected in the OB with 1 μL of quinolinate 45 mM (quino45, $n = 6$) or 90 mM (quino90, $n = 6$); and animals which received a saline injection in the OB (sham, $n = 7$) (Table 1). Twelve other male Sprague-Dawley rats (300 g) were also involved in a preliminary study using laser Doppler flowmetry (LDF) to optimize the doses of quinolinate. Animal experiments were performed in strict accordance with the recommendations of the EEC (86/609/EEC) and ethical standards of the statutory order 87,848 (October 13, 1987) of the French Ministry of Agriculture (authorization no 91-166).

Validation of Active Quinolinate Doses by Laser-Doppler Flowmetry

The excitotoxic effect of each dose of quinolinate was further validated in the OB on the basis of dose response curves established by LDF. Indeed, because of the robust coupling between the neuronal activity and cerebral blood flow (CBF), local changes in CBF can be used as a reliable index of neuronal activity. These changes can be measured using LDF, a method that measures relative changes in blood flow by calculating the Doppler shift imparted to remitted illumination by moving red blood cells. An increase in red blood cell velocity results in an increase in LDF. In this study, LDF recordings were performed in the OB with a LDF probe (500 μm in diameter, OxylFlo™, Oxford Optronics, Oxford, UK) lowered in the ventral OB (18). Local CBF data were collected continuously at a frequency of 2 Hz and were averaged on a second or minute basis. Local CBF was evaluated after quinolinate injections and physiological stimulations. Animals were anesthetized during the whole procedure by an intraperitoneal injection of ketamine (Imalgene 500®, Rhone-Poulenc Merieux; 100 mg/kg) and medetomidine (Domitor®, Pfizer santé Animale; 0.5 mg/kg). We chose ketamine over isoflurane because the overall LDF procedure took 4 to 5 h and required a deeper anaesthetic state. In addition, rats recovered very well after ketamine anaesthesia. For the physiological stimulation, three amylacetate (banana smell, 5% vapor pressure) puffs were presented for a duration of 8 s to the animal and compared to air ($n = 2$ rats, 3 trials per rat). For the excitotoxic stimulations, we performed successive injections of 1 μL of quinolinate 25, 45, and 90 mM ($n = 2$ rats per group) for 2 min. Injections were performed via a cannula attached to the laser Doppler probe.

Surgery to Induce Excitotoxic Lesions

Animals were anesthetized using isoflurane (Forène®, Abbott France, 3% for induction and 1–1.5% for maintenance) to perform quinolinate injections into the OB. This anesthetic regime is well-suited for brief surgery procedures (<1 h) and allows for very good recovery in the animals. Surgery was performed by using a stereotaxic apparatus (Stoelting, Wood Dale). Excitotoxic lesions were induced bilaterally by injecting 1 μL of quinolinate at 90 or 45 mM into the ventral OB at the following stereotaxic coordinates with respect to bregma: Anterior posterior (AP) = +6.7 mm; medial-lateral (ML) = ±1.2 mm; dorsal-ventral (DV) = −2.2 mm. Quinolinate is a neurotoxin that selectively activates NMDA receptors (13,14) and leads to profound changes in the brain tissue such as neuronal death, and hyperactivation of astroglia and microglial cells (19). Previous studies in our laboratory have shown that, in the striatum, 24 h post-injection of 1 μL of quinolinate at 45 mM and more, 100% of the animals present excitotoxic lesions characterized in particular by TUNEL (the terminal deoxynucleotidyl transferase-mediated biotinylated uridine triphosphate nick end labeling)-positive (apoptotic) cells. The doses of quinolinate used in this study were thus chosen on the basis of this previous report (14) and were confirmed in the OB by LDF recordings during neurotoxin injection.

Design of the MEMRI Study

The general protocol of the MEMRI study is described in Table 1. On day 1, all the animals were subjected to a baseline MRI scan, that is, without any Mn^{2+} administration. On day 2, quinolinate-injected and sham animals underwent surgery and received 1 μL of saline, quinolinate 45 mM or quinolinate 90 mM, respectively. Control animals did not undergo surgery or odor stimulation. Day 3, the last day of the experiment, was dedicated to MEMRI. A $MnCl_2$ solution (5 μL, 1 M) was injected using a catheter into the naris of all animals which were

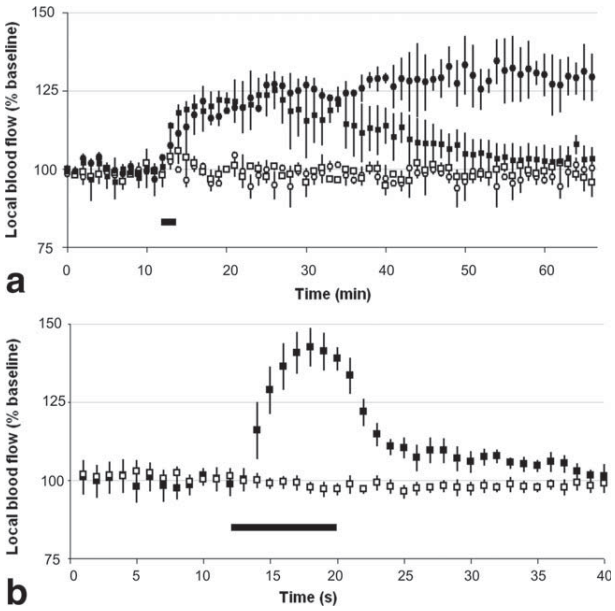

FIG. 1. Laser Doppler flowmetry (LDF) in the ventral OB following physiological or excitotoxic stimulations. **a**: Quinolinate-induced increases in local cerebral blood flow (CBF) at different doses. Open circle: saline; open square: quinolinate 25 mM; black square: 45 mM; black circle: quinolinate 90 mM injection. The horizontal bar represents the duration of quinolinate injection (2 min). Quinolinate did not induce any significant activation at 25 mM. At 45 mM, the increase in local CBF was maintained for approximately 30 min. It was maintained over the recording time (50 min) with 90 mM. **b**: The odor-induced increases in the local CBF induce an activation that last for approximately 10 s after the amylacetate presentation. The horizontal bar represents the duration (8 s) of odor or air presentation. Open square: air; black square amylacetate. Each point of the graphs represents mean ± s.e.m.

lightly anesthetized with isoflurane. Ten minutes post-recovery from anaesthesia, the animals from the odor stimulation group were exposed to amylacetate for 20 mins using 30 s on/off pulses. Then, the animals were left awake in their cage environment for 50 mins. Animals from all other groups were not exposed to odor and were left awake in their cage for 80 min following Mn^{2+} administration. For MEMRI, all rats were anaesthetized with an intraperitoneal injection of a mixture containing ketamine (100 mg/kg) and medetomidine (0.5 mg/kg) which represented a long term anaesthetic procedure. MEMRI images were recorded at three time points (90, 150, and 200 min) post-Mn^{2+} administration. As axonal transport of Mn^{2+} is dependent on body temperature (20), the animal's temperature was maintained during anaesthesia by a circulating hot-water blanket.

MRI Acquisition and Data Analysis

MR images of the OB were recorded using a 3 T spectrometer (MAGNETON Trio MR, Siemens) with a human elbow four-channel phase array coil (Siemens flex small). T1-weighted 3D images were recorded using gradient echo sequences (Resolution = 250 × 250 × 500 μm^3, Field of View = 32 × 32 × 32 mm^3, Matrix = 128 × 128 × 64, repetition and echo times (TR/TE) = 11/4 ms, alpha = 9°, number of averages = 32, acquisition time = 37 min). A tube of water was fixed above the head of the scanned rat to provide a reference signal for each scan. Mn^{2+}-related signal enhancement was evaluated on one MRI slice located at the level of the anterior OB. Image analysis was based on the method previously reported by Pautler and Koretsky (10). For each animal, regions of interest (ROIs) were defined on images recorded 200 min post-Mn^{2+} injection, in lateral and medial sides of the right and left OBs. These regions correspond to superficial layers where the functional units (olfactory glomeruli) are located and receive projections from the olfactory nerve layer. Based on the ROIs identified at 200 min, corresponding ROIs were reported at 90 and 150 min scans and at the pre-Mn^{2+} injection scan. The intensity of the signal in a given ROI was divided by the intensity of the signal in the water tube (reference signal) that was localized on the top of the nose, just above the OB. This provided a normalized signal for each MR scan. The signal enhancement at a given time after Mn^{2+} administration for a rat was evaluated as the percentage of normalized signal increase at this given time as compared to the baseline scan for the same rat.

Histology

For the histological study, rats from the sham and quino90 groups were sacrificed with a pentobarbital overdose and their brains were removed and frozen at −40°C in isopentane. Brain sections (20 μm) were post-fixed in PFA 4% for 60 min and washed in PBS. Immunolabelling of sections was performed with an automated immunostaining system (Ventana Discovery XT Medical System S.A, Illkirch, France). Sections were first treated with a heat induced antigen retrieval technique in citrate buffer (pH 6), and then incubated for 60 min in a primary antibody solution: anti-NeuN, 1:1000 dilution (Chemicon International, Temecula, CA) and antiglial fibrillary acidic protein (GFAP), 1:5000 dilution (DakoCytomation, Glostrup, Denmark). Sections were then processed by the avidin-biotin peroxidise complex and DAB chromophore, followed by a hematoxylin staining (counterstaining technique).

The density of neurons (NeuN staining) and astrocytes (GFAP staining) were evaluated by using image J (http://imagej.nih.gov/ij/). Three high magnification images (×60) were recorded in the mitral and granule cell layers from each hemisphere of sham and quino90 rats. The color information from the images was deconvolved ("Color Deconvolution/FastRed FastBlue DAB" plugin) to extract a new image specific of the DAB chromophore (21). NeuN and GFAP positive cells were then selected ("threshold/isodata" tool) and their density was evaluated ("analyze particles" tool).

Statistical Analysis

The overall signal difference from 0 to 200 min time points was analyzed using a two-factors ANOVA with repeated measures (with "group" as the between-subjects factor and "time following Mn^{2+} administration" as the within-subject factor) using Statistica v7 software (StatSoft,

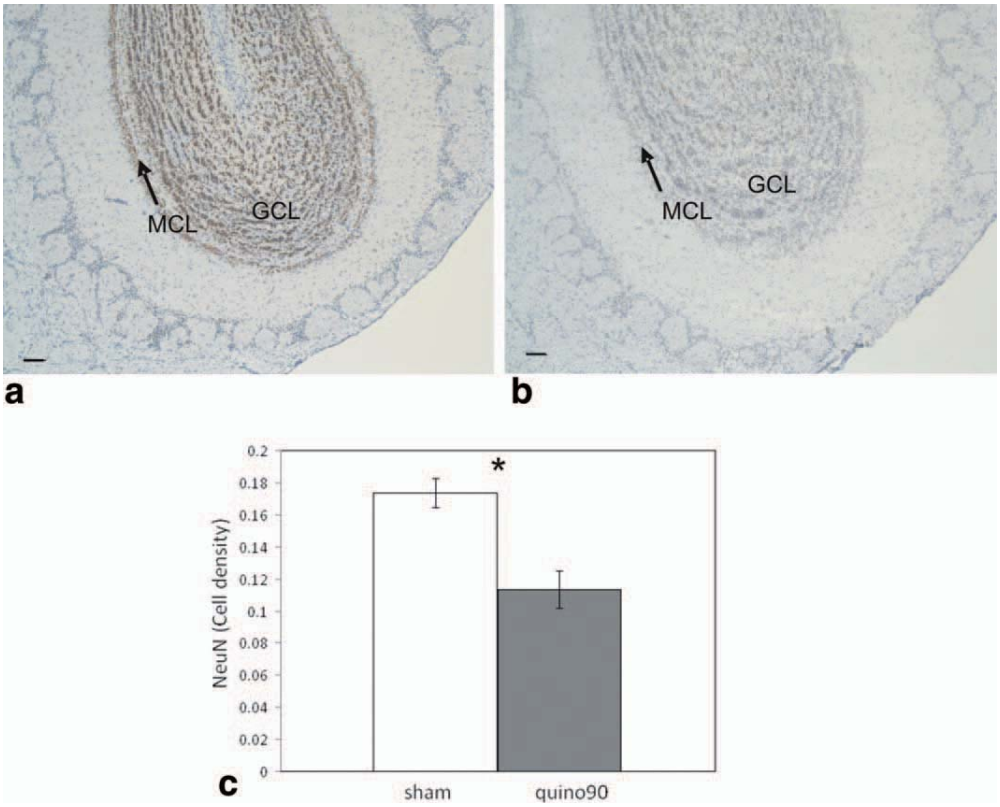

FIG. 2. NeuN immunohistochemical staining of OB sections of sham (**a**) and "quino90" (**b**) rats 24 h post-surgery. **c**: There was a significant reduction of cell density in the mitral and granular cell layers (MCL and GCL) in rats from the "quino90" group (b) compared to sham animals (a) (Mann Whitney's test, $P < 0.005$). Scale bar: 100 μm. [Color figure can be viewed in the online issue, which is available at wileyonlinelibrary.com.]

Tulsa, OK). The signal changes were further analyzed by evaluating early (time zero to first MEMRI image at 90 min post-Mn^{2+} injection) and late (from 90 to 200 min post-Mn^{2+} injection) phases. Signal changes during early and late phases were estimated using one-factor ANOVA. Quantifications from histological data were analyzed by using Mann-Whitney's tests. A value of $P < 0.05$ was considered to be a significant effect. All data are presented as the mean ± standard error of the mean (s.e.m).

RESULTS

Quinolinate Induces Strong Activation in the OB and Associated Excitotoxic Effects

Figure 1a shows local CBF changes in response to local injection (2 min duration) of different doses of the neurotoxin quinolinate. For quinolinate 25 mM no increases in the LDF signal could be observed. For quinolinate 45 mM, CBF reached a peak (∼ 30% of baseline) before returning to baseline 50 min post-injection. For quinolinate 90 mM, CBF increased durably and did not return to baseline 50 min post-injection. Since a strong and sustained increase of excitatory activity is necessary to induce excitotoxicity, the doses of 45 and 90 mM were selected for our MEMRI experiments. Figure 1b displays the time course of local CBF recorded by LDF in the OB to 10 s odor stimulation with 5% amylacetate: odor-evoked increases in CBF were rapid, reached a peak (∼ 40% of baseline) and stopped by the end of the sensory stimulation.

Histological studies confirmed excitotoxic lesions in the quinolinate-injected animals. Indeed, we observed a significant loss of the neuronal marker NeuN of the quinolinate-injected animals as compared to sham rats (Fig. 2, $U = 2$, $P < 0.005$). Twenty-four hours after the administration of quinolinate, GFAP immunohistochemistry did not reveal any significant changes of the shape or density of astrocytes (Fig. 3a–c, U = 16, ns). An activation of the astrocytes was however obvious 72 h after the administration of quinolinate (Fig. 3d).

MEMRI Signal Follow-Up in Excitotoxic and Physiological Conditions

MEMRI was characterized after intranasal Mn^{2+} administration (Fig. 4a–e), in both physiological and excitotoxic conditions, in regions corresponding to the superficial layers of the rostral OB, i.e., at the level of the olfactory nerve and glomerular layer (2,10,22). Intranasal Mn^{2+} administration led to time-dependent MEMRI signal increases (Fig. 4f; for all groups ANOVA [$F(3, 75) = 246$, $P < 0.001$] and post hoc analysis within each group: all $P < 0.001$). This result indicates that Mn^{2+} was taken up and transported into the OB. The overall signal uptake from 0 to 200 min time points was higher in the excitotoxic conditions ("quino90" group) as compared to the

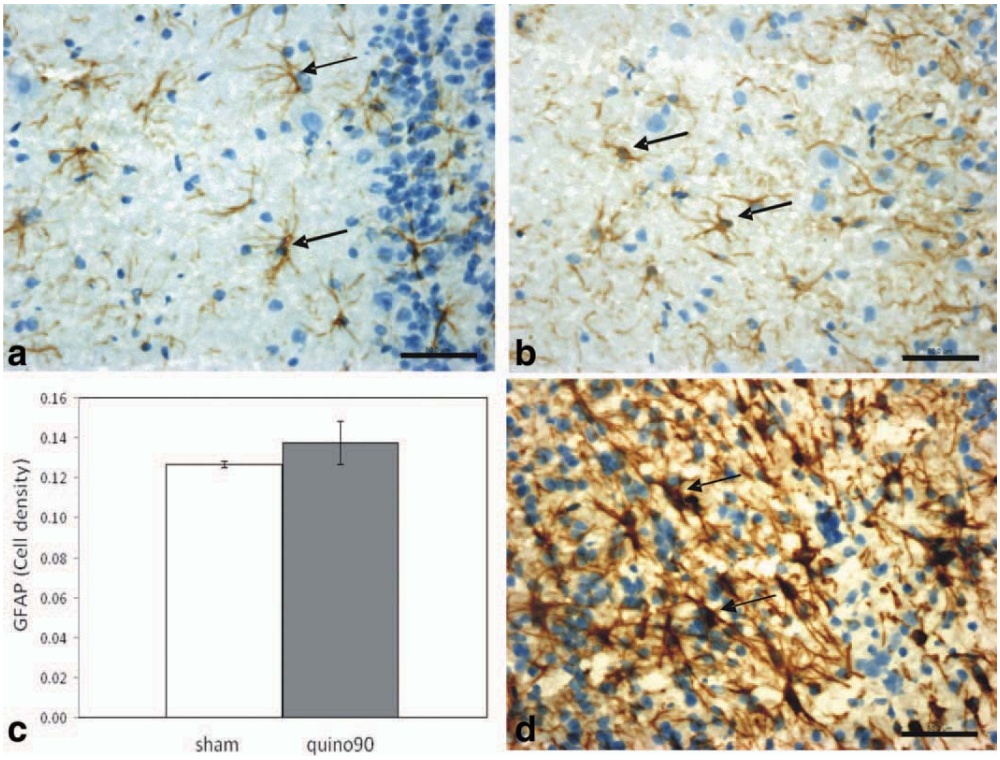

FIG. 3. GFAP immunohistochemical staining of OB sections in sham (**a**) and quino90 rats 24 (**b**) and 72 h (**d**) post-surgery. No significant changes of the astrocyte shape (a-b, arrows) or density (**c**) was detected 24 h post-surgery. The density and shape of astrocytes were however modified 72 h post-quinolinate injections (b–d, arrows). Scale bars: 50 μm. [Color figure can be viewed in the online issue, which is available at wileyonlinelibrary.com.]

sham group (post hoc analysis, [$F(1,25) = 9.7$, $P < 0.005$]; Fig. 4f). The signal in the "quino45" group showed an intermediate intensity in between quino90 and sham rats.

In addition to the increased MEMRI signal in the excitotoxic conditions, we found a higher signal in the physiological stimulation ("odor-stim" group) as compared to the control group (post hoc analysis, $F(1,25) = 6.9$, $P < 0.02$]; Fig. 4f). Interestingly, the MEMRI signal was similar in the "quino90" and "odor-stim" groups (post hoc analysis, n.s.; Fig. 4f).

To further characterize the MEMRI signal in excitotoxic versus physiological conditions, we performed a second analysis focused on the signal time course splitting recording time into early (time zero to first MEMRI image acquired at 90 min post-Mn^{2+} injection) and late (from 90 to 200 min post-Mn^{2+} injection) phases (Fig. 5). For the early phase corresponding to Mn^{2+} entry in the OB cells, a one factor ANOVA revealed a significant difference between the slopes of the signal increase in different groups [$F(4,25) = 4.4$, $P < 0.01$]. Post hoc analysis revealed a significant difference between the activated groups ("odor-stim" and "quino90") versus the control and sham groups ($P < 0.05$). On the contrary, for the late phase, a one factor ANOVA did not reveal any difference between these groups [$F(4,25) = 1.2$, n.s.]. This result indicates that the dynamics of the MEMRI signal are determined by the entry of Mn^{2+} in the early phase during the Mn^{2+} loading of the OB cells.

DISCUSSION

In this study, we investigated the MEMRI signal following the induction of excitotoxicity induced by the NMDA receptor agonist quinolinate injected into the OB. Our results, determined by LDF and histology, indicate that at high doses, quinolinate strongly increases local activity which is maintained over time and leads to excitotoxicity. Our MRI study showed that the MEMRI signal intensity associated with these excitotoxic events is significantly increased (Fig. 4). We suggest that two opposite neuroglial mechanisms can be implicated in determining the increase of MEMRI signal in this lesioned area. First, considering the neuronal loss induced 24 h post-quinolinate administration (Fig. 2), we should have seen a decrease of the MEMRI signal accompanying this neuronal damage because of a decrease in the number of Mn^{2+} uptake sites. However, this was not the case because opposite mechanisms to this decrease were also triggered. Glutamate receptor-mediated excitotoxicity is associated with an elevation of cytosolic Ca^{2+} concentration and an increase in the entry of Ca^{2+} into neurons (14,15). This mechanism is still triggered in surviving neurons and can compensate for the signal decrease due to neuronal loss. Glial reaction might be an alternative explanation to the increased MEMRI signal seen in our experiments. Indeed, previous studies have shown that, after a cerebral insult, Mn^{2+} can accumulate in microglia (3) and in astrocytes with concentrations which are 10–50-fold greater than in neurons (23) leading to strong

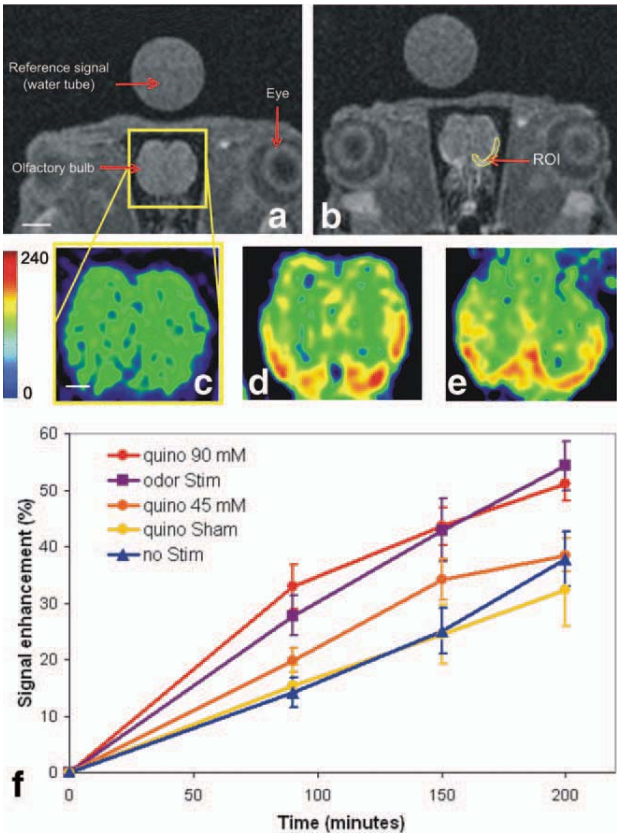

FIG. 4. Odor- versus quinolinate-evoked MEMRI signals in the rat OB. **a,b**: T1-weighted MR coronal images of the OB, during baseline (a) and 200 min post-Mn^{2+} injection (b). Signal intensity is calculated relative to the reference from the water tube above the head of the rat. **c–e**: MEMRI signal, before Mn^{2+} (c), 200 min post-Mn^{2+} with olfactory stimulation (d), and with local quinolinate injection (e). The signal increases with both stimulations. MR images are pseudo-colored so that enhanced signal appears in red (color scale is in arbitrary unit). Scale bar 3 mm for (a,b) and 1 mm for (c–e). **f**: Changes in % of MR signal enhancement across time intervals (mean ± s.e.m.), *: $P < 0.05$.

MEMRI signal increase (3). In our experiments, the density of reactive astrocytes was not significantly increased at 24 h post-lesion (Fig. 4). However, we detected a strong staining for GFAP-immunoreactive astrocytes 72 h after quinolinate injection. Our data are consistent with a previous report showing the same time course for GFAP immunoreaction after quinolinate injection (24). This suggests that an activation process had already started 24 h after quinolinate injection. In addition, metabolic activation (fluoro-deoxyglucose uptake) of astrocytes is reported even 1 h after quinolinate injection (14). We can thus not rule out a significant participation of glial cells in the MEMRI signal.

In the second part of this work, we took advantage of the OB features to investigate the physiological changes of the MEMRI signal after odor stimulation. In accordance with previous studies (10), we have shown that MEMRI is an efficient imaging technique to map odor-induced activities. Indeed, we observed that MEMRI can detect amylacetate-induced physiological activations of specific areas located in the lateral and ventral parts of the OB.

How can we interpret physiological and pathological mechanisms associated with MEMRI signal modifications in the OB? The olfactory glomeruli where the MEMRI signal was detected are the functional modules of the OB. They receive projections from olfactory receptor neurons (25). Within glomeruli, the sensory neurons make excitatory synapses onto the dendrites of postsynaptic neurons (mitral cells). The glomeruli thus contain the first synaptic network of the olfactory system. Once injected in the naris, Mn^{2+} was taken up and moved from the naris to the presynaptic terminals of the glomeruli via anterograde transport within axons of the olfactory nerve (26). The fast anterograde transport that is used for Mn^{2+} transportation has a speed of 3.6 to 18 mm/h (27). Because of the small distance between the olfactory epithelium and the glomeruli, one can consider that during our first imaging time (90 min), Mn^{2+} had reached and accumulated into the glomerular synapses. During the physiological sensory stimulation, i.e., in the "odor-stim" group, we found an increased uptake of Mn^{2+}. This can be explained by an increased release of Mn^{2+} from the olfactory neurons presynaptic terminals. Indeed, during physiological activation, glutamate activates its postsynaptic receptors on mitral cells including the ionotropic AMPA and NMDA (28) and the metabotropic mGluR receptors (29), all of them triggering the depolarization of the cell membrane thus leading to VGCC activation. Mn^{2+} thus enters the postsynaptic cells in the olfactory glomeruli via NMDA receptors and VGCC. During excitotoxic events, ionotropic (NMDA-subtype) and metabotropic glutamate receptors (15) are

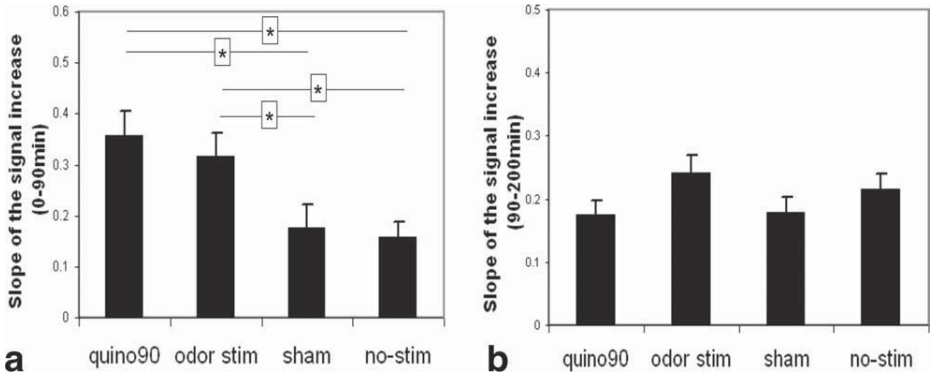

FIG. 5. Changes in the slope of the MEMRI signal during early (time zero to 90min post-Mn^{2+} injection, (**a**)) and late (from 90 to 200 min post-Mn^{2+} injection (**b**)) phases following $MnCl_2$ administration. In the early phase, increases in the signal slope were higher in the activated groups ("odor-stim" and "quino90") as compared to the control and sham groups.

also activated which can increase the entrance of Mn^{2+} in the postsynaptic cells. These mechanisms can explain why, when compared to excitotoxic injury, the physiological activation revealed an identical enhancement of the MEMRI intensity. To further characterize putative differences between the groups we analyzed the time course of the MEMRI signal. In both conditions, we have shown that the dynamics of the MEMRI signal are equal and are determined by early and not late phases following manganese injection. Future work on detangling the cellular origins of MEMRI signal in physiological and excitotoxic conditions is required. For example, an interesting perspective of this study would be to investigate by pharmacology the effect of a NMDA antagonist (i.e., MK801) on the MEMRI signal in normal versus excitotoxic conditions. This could help evaluate the specific participation of NMDA receptors versus the metabotropic glutamate receptors (9,15) in the quinolinate-induced neurodegeneration model.

As a conclusion, we have shown that, in addition to the evaluation of physiological neuronal activation, MEMRI can be used to follow-up excitotoxic events in vivo. Importantly, since models of neurodegenerative diseases present excitotoxicity in precise brain circuits (12), an exciting perspective of our work is to use MEMRI as an integrative tool to follow the dynamics of neuropathological mechanisms over time.

ACKNOWLEDGMENTS

The authors thank Gilles Bonvento for advice on LDF recordings, Emmanuel Brouillet for advice on quinolinate usage and for comments on the article, and Philippe Hantraye and Carsten Ehrhardt for their support of this work. Hirac Gurden and Marc Dhenain contributed equally to this work.

REFERENCES

1. Koretsky AP, Silva AC. Manganese-enhanced magnetic resonance imaging (MEMRI). NMR Biomed 2004;17:527–531.
2. Pautler RG, Silva AC, Koretsky AP. In vivo neuronal tract tracing using manganese enhanced magnetic resonance imaging. Magn Reson Med 1998;40:740–748.
3. Widerøe M, Olsen O, Pedersen TB, Goa PE, Kavelaars A, Heijnen C, Skranes J, Brubakk AM, Brekken C. Manganese-enhanced magnetic resonance imaging of hypoxic-ischemic brain injury in the neonatal rat. Neuroimage 2009;45:880–890.
4. Aoki I, Wu YJL, Silva AC, Lynch RM, Koretsky AP. In vivo detection of neuroarchitecture in the rodent brain using manganese-enhanced MRI. Neuroimage 2004;22:1046–1059.
5. Gilad AA, Walczak P, McMahon MT, Na HB, Lee JH, An K, Hyeon T, van Zijl PC, Bulte JW. MR tracking of transplanted cells with "positive contrast" using manganese oxide nanoparticles. Magn Reson Med 2008;60:1–7.
6. Canals S, Beyerlein M, Keller AL, Murayama Y, Logothetis NK. Magnetic resonance imaging of cortical connectivity in vivo. Neuroimage 2008;40:458–472.
7. Van der Linden A, Van Meir V, Tindemans I, Verhoye M, Balthazart J. Applications of manganese-enhanced magnetic resonance imaging (MEMRI) to image brain plasticity in song birds. NMR Biomed 2004; 17:602–612.
8. Lin YJ, Koretsky AP. Manganese ion enhances T1-weighted MRI during brain activation: an approach to direct imaging of brain function. Magn Reson Med 1997;38:378–388.
9. Itoh K, Sakata M, Watanabe M, Aikawa Y, Fujii H. The entry of manganese ions into the brain is accelerated by the activation of N-methyl-D-aspartate receptors. Neuroscience 2008;154:732–740.
10. Pautler RG, Koretsky AP. Tracing odor-induced activation in the olfactory bulbs of mice using manganese-enhanced magnetic resonance imaging. Neuroimage 2002;16:441–448.
11. Yu X, Zaim Wadghiri Y, Sanes DH, Turnbull DH. In vivo auditory brain mapping in mice with Mn-enhanced MRI. Nat Neurosci 2005; 8:961–968
12. Lipton SA. Excitotoxicity. In: Bähr M, editor. Neuropretection models, mechanisms and therapies. Weinheim: Wiley-VCH; 2004. pp 291–313.
13. Stone TW, Addae JI. The pharmacological manipulation of glutamate receptors and neuroprotection. Eur J Pharmacol 2002;447:285–296.
14. Jacquard C, Trioulier Y, Cosker F, Escartin C, Bizat N, Hantraye P, Cancela JM, Bonvento G, Brouillet E. Brain mitochondrial defects amplify intracellular [Ca2+] rise and neurodegeneration but not Ca2+ entry during NMDA receptor activation. FASEB J 2006;20: 1021–1023.
15. Lisý V, Stastný F. Nitric oxide synthase inhibition and glutamate binding in quinolinate-lesioned rat hippocampus. Physiol Res 2002; 51:299–307.
16. Stanika RI, Pivovarova NB, Brantner CA, Watts CA, Winters CA, Andrews SB. Coupling diverse routes of calcium entry to mitochondrial dysfunction and glutamate excitotoxicity. Proc Natl Acad Sci USA 2009;106:9854–9859.
17. Serrano F, Deshazer M, Smith KD, Ananta JS, Wilson LJ, Pautler RG. Assessing transneuronal dysfunction utilizing manganese-enhanced MRI (MEMRI). Magn Reson Med 2008;60:169–175.
18. Shiba K, Machida T, Uchida S, Hotta H. Sympathetic neural regulation of olfactory bulb blood flow in adult and aged rats. Auton Neurosci 2009;147:75–79.
19. Pierozan P, Zamoner A, Soska AK, Silvestrin RB, Loureiro SO, Heimfarth L, Mello e Souza T, Wajner M, Pessoa-Pureur R. Acute intrastriatal administration of quinolinic acid provokes hyperphosphorylation of cytoskeletal intermediate filament proteins in astrocytes and neurons of rats. Exp Neurol 2010;224:188–196.
20. Smith KD, Kallhoff V, Zheng H, Pautler RG. In vivo axonal transport rates decrease in a mouse model of Alzheimer's disease. Neuroimage 2007;35:1401–1408.
21. Ruifrok AC, Johnston DA. Quantification of histochemical staining by color deconvolution. Anal Quant Cytol Histol 2001;23:291–299.
22. Chuang KH, Lee JH, Silva AC, Belluscio L, Koretsky AP. Manganese enhanced MRI reveals functional circuitry in response to odorant stimuli. Neuroimage 2009;44:363–372.
23. Erikson KM, Aschner M. Increased manganese uptake by primary astrocyte cultures with altered iron status is mediated primarily by divalent metal transporter. Neurotoxicology 2006;27:125–130.
24. Dihné M, Block F, Korr H, Töpper R. Time course of glial proliferation and glial apoptosis following excitotoxic CNS Injury Brain Res 2001;902:178–189.
25. Shepherd GM, Greer CA. The olfactory bulb. In: Shepherd G, editor. The synaptic organization of the brain, 4th ed. New York: Oxford University Press; 1998. pp 159–203.
26. Bearer EL, Falzone TL, Zhang X, Biris O, Rasin A, Jacobs RE. Role of neuronal activity and kinesin on tract tracing by manganese-enhanced MRI (MEMRI). Neuroimage 2007;37(Suppl 1):S37–S46.
27. Roy S, Zhang B, Lee VM, Trojanowski JQ. Axonal transport defects: a common theme in neurodegenerative diseases. Acta Neuropathol 2005;109:5–13.
28. Carlson GC, Shipley MT, Keller A. Long-lasting depolarization in mitral cells of the rat olfactory bulb. J Neurosci 2000;20:2011–2021.
29. Ennis M, Zhu M, Heinbockel T, Hayar A. Olfactory nerve-evoked, metabotropic glutamate receptor-mediated synaptic responses i n rat olfactory bulb mitral cells. J Neurophysiol 2006;95:2233–2241.